American Mineralogist, Volume 72, pages 902–913, 1987

Distribution of trace transition elements in olivine and pyroxenes from ultramafic xenoliths: Application of microprobe analysis

Jean-Louis Bodinier, Claude Dupuy
Centre Géologique et Géophysique, USTL, Place E. Bataillon, 34060 Montpellier Cedex, France
Jarda Dostal
Department of Geology, Saint Mary's University, Halifax, Nova Scotia B3H 3C3, Canada
Claude Merlet
Service Commun Microsonde, USTL, Place E. Bataillon, 34060 Montpellier Cedex, France

Abstract

Microprobe analyses of transition elements (Ti, Cr, Mn, Co, Ni, and Zn) in coexisting olivine, orthopyroxene, and clinopyroxene of peridotite xenoliths from kimberlites and alkali basalts are used to estimate olivine/pyroxene and clinopyroxene/orthopyroxene partition coefficients. The analyzed samples include garnet peridotite, spinel peridotite, and spinel-plagioclase peridotite. In olivine, a concentration gradient for transition elements appears only in the outermost part of the crystals and is probably related to a late thermal event. The cores of the pyroxenes are rather homogeneous for the analyzed elements except Cr and to a lesser extent Ti. The partition coefficients vary with pressure, temperature, and mineral composition. The partitioning of Ti between olivine and pyroxenes may be a sensitive indicator of the pressure of equilibration.

Introduction

There are two drawbacks associated with using separated minerals in trace-element analyses. First, the minerals generally contain impurities, and second, the variations within individual crystals, which are of prime importance in understanding petrogenetic processes, are obliterated. These difficulties may be overcome by the use of an ion microprobe (e.g., Shimizu, 1978; Shimizu and Allègre, 1978; Suzuki, 1981). Alternatively, an electron microprobe may also provide quantitative analyses of relatively low concentration levels (Bence et al., 1980; Bizouard, 1982), but the data produced by this method are rather scarce (Bishop et al., 1978; Delaney et al., 1979; Hervig et al., 1980; Delano, 1986; McKay, 1986).

This study reports electron-microprobe analyses of several minor and trace transition elements in olivine and pyroxenes from six peridotite xenoliths. The element distribution within each mineral and between samples is presented, and the variations of partition coefficients are discussed in the light of the *P-T* conditions of equilibration of the rocks. The influence of the major-element composition of the minerals is also evaluated.

Sample description

Two garnet peridotites, three spinel peridotites, and a spinel-plagioclase peridotite were selected for the study to include a large range of *P-T* equilibration conditions. The garnet peridotites (samples PHN-1611 and PHN-1569) are xenoliths in kimberlite from Lesotho studied by Nixon and Boyd (1973), Boyd and Finger (1975), and Delaney et al. (1979). The four others are inclusions scavenged by alkali basalts in Cameroon (sample CAM-2B), southern Algeria (sample MAN 91-1), and southern France (samples C 80-335 and LEZ-1). A description of the petrography and the major-element composition of the mineral phases of the samples from Cameroon and Algeria was published by Dautria and Girod (1986) and Girod et al. (1981), respectively. The xenoliths from southern France were collected from two localities (Table 1) and described by Coisy (1977) and Berger (1981). The textures of the samples and the estimated *P-T* conditions of equilibration are given in Table 1, and the main major-element characteristics of the minerals are reported on Tables 4 to 7 together with the trace-element data. None of the analyzed samples contains exsolution lamellae in pyroxene, with the exception of sample CAM-2B, which has a minor amount of exsolved spinel.

Analytical procedure

The analyses were performed with an automated Camebax microprobe operating at 30 kV and 100 nA. The beam size was fixed at 2 μm in diameter, and the determination of the trace transition elements was done on the $K\alpha$ line employing LiF and PET crystals. The major elements were analyzed at the same time for matrix corrections, using the Cameca ZAF routine. The standards (Table 2) were analyzed with a beam current lower than that used for the samples. The background, free of interference and corrected from absorption edge effect, was interpolated from symmetrical or asymmetrical measurements on each side of the peaks, at variable distances according to the elements.

The data were processed on a PDP 11 computer using a program adapted by one of us (C.M.). The program performs data collection and processing with a deconvolution procedure for overlapping peaks and filtering adapted from Statham (1977), Wittry (1980), and Armigliato et al. (1982). The statistical error is related to the counting time; as with the detection limit, this

0003–004X/87/0910–0902$02.00

TABLE 1. Petrographic characteristics and estimated *P-T* conditions for the xenoliths

Sample and reference	Name	Texture		*T* (°C)* W	B	F	*P* (kbar)
PHN-1611 Nixon and Boyd (1973)	garnet lherzolite	fluidal mosaic	(C) (R)	1320 1320	1435 1435		62†
PHN-1569 Nixon and Boyd (1973)	garnet harzburgite	coarse granular	(C) (R)	905 915	895 910	980 1000	30†
C 80-335 Berger (1981)	spinel lherzolite	porphyroclastic	(C) (R)	1115 1140	1170 1200	1065 1140	23‡
MAN 91-1 Girod et al. (1981)	spinel lherzolite	coarse tabular	(C) (R)	945 950	895 905	890 910	13‡
LEZ-1 Coisy (1977)	clinopyroxene harzburgite	coarse equant, slightly porphyroclastic	(C) (R)	920 955	865 920	860 905	12‡
CAM-2B Dautria and Girod (1986)	spinel and plagioclase lherzolite	porphyroclastic	(C) (R)	900 970	895 940	960 960	6§

* Temperatures calculated from core (C) and rim (R) of minerals by using the following geothermometers: W, Wells (1977); B, Bertrand and Mercier (1986); F, Fabriès (1979).
† Pressure estimates taken from Sotin et al. (1987).
‡ Pressures evaluated by projecting the temperature estimates onto the oceanic geotherm (e.g., Mercier and Carter, 1975), which is likely to represent the French Massif Central and Hoggar geotherms at the time of the volcanism (Girod et al., 1981; Lucazeau and Bayer, 1982; Nicolas et al., 1987).
§ Temperature estimate projected on the transition limit of spinel and plagioclase stability fields (Gasparik, 1984).

parameter is strongly dependent upon the type of mineral analyzed. The detection limits calculated according to the method of Ancey et al. (1978), the counting time and the statistical error (coefficient of variation) for Ti, V, Cr, Mn, Co, Ni, Zn in orthopyroxene and Ca, Ti, Cr in olivine are reported in Table 2. The accuracy may be partly assessed by comparing analyses of samples PHN-1611 and PHN-1569 with those obtained elsewhere either by electron or ion microprobe (Table 3).

In each sample, about 70 analyses were performed along a profile from the core to the rim in three to four pairs of adjacent minerals (olivine-orthopyroxene, orthopyroxene-clinopyroxene, clinopyroxene-garnet). The analyses of the rim were made at a distance of 10 μm from the grain boundary. The influence of secondary fluorescence on rim analyses (e.g., McKay, 1986) was negligible for most elements, except Cr in olivine adjacent to spinel. In the latter case the measurement was made after masking spinel: in sample LEZ-1 (Table 4), the apparent Cr concentration in the olivine rim was about 1500 ppm before masking and 538 ppm after masking.

ELEMENT VARIATIONS

1. Variations of individual minerals among the different xenoliths

This variation is shown by the average contents of the core of the minerals (Tables 4, 5, and 6). With increasing forsterite content of olivine, the Ni concentration increases and Mn decreases (Table 4), in agreement with the diadochy between Mg-Ni on the one hand and Fe^{2+}-Mn^{2+} on the other. One exception is olivine of sample PHN-1611, which has low Mn but high Ni contents compared to the other samples. This olivine and that of sample C 80-335 have significantly higher Ca and Cr contents than the others, probably because of their high temperature of equilibration (e.g., Kushiro et al., 1972). In fact, it has been shown that the Ca content of olivine increases with the temperature and decreases with the pressure

TABLE 2. Analytical parameters for orthopyroxene and olivine from sample PHN-1611

Element	Concentration (ppm)	Standard	Counting time* (s) Peak	Background	Detection limit (ppm)	Statistical error† (%) (1)	(2)
			Orthopyroxene				
Ti‡	1099‡	TiO_2	138	71	5	3.4	7.2
V‡	60†	Vanadinite	210	180	6	2.1	5.1
Cr‡	1373	Cr_2O_3	66	33	10	3.6	7.5
Mn‡	988	Rhodonite	86	53	15	3.1	6.6
Co§	89	Co	440	430	7	9.3	21.0
Ni§	1068	Ni	150	100	26	2.0	4.5
Zn§	54	ZnO	350	300	24	23.0	53.0
			Olivine				
Ca‡	1353	Wollastonite	105	95	26	6.9	15.0
Ti‡	158	TiO_2	135	115	4	15.0	35.0
Cr‡	189	Cr_2O_3	145	125	6	10.4	24.0

* Total counting time, major + trace elements, peak + background: 900 s.
† Statistical errors calculated after the procedures of (1) Ziebold (1967) and (2) Ancey et al. (1978).
‡ Crystal: PET.
§ Crystal: LiF.

TABLE 3. Comparison of transition-element microanalyses in mineral phases of samples PHN-1611 and PHN-1569

	Olivine PHN-1611	Ortho-pyroxene PHN-1611	Clino-pyroxene PHN-1611	Clino-pyroxene PHN-1569
Ti	175 (A)	1334–1380 (A)	2176–2228 (A)	20–141 (A)
	156 (B)	1224 (B)	1860 (B)	60 (B)
		1260–1380 (C)		
			1680 (E)	90 (E)
V			150–154 (A)	218–250 (A)
			110 (E)	190 (E)
Cr	230 (A)	940–1440 (A)	3503–3851 (A)	10345–12263 (A)
	281 (B)	1498 (B)		8894 (B)
		960–1500 (C)		
	275 (D)	1476 (D)	3624 (D)	
			2400–3120 (E)	8880 (E)
Mn	962 (A)	986–1012 (A)	1038–1063 (A)	491–527 (A)
	960 (B)	1007 (B)	875 (B)	511 (B)
			810 (E)	500 (E)
Co			64–67 (A)	15–17 (A)
			50 (E)	28 (E)
Ni	3047 (A)	999–1055 (A)		
	2782 (B)	817 (B)		
	2900 (C)	1020–1100 (C)		

Note: Electron microprobe—(A) this study, (B) Delaney et al. (1979), (C) Smith and Boyd (1987), (D) Hervig and Smith (1982); ion microprobe—(E) Shimizu and Allègre (1978).

(Finnerty and Boyd, 1978; Adams and Bishop, 1982). The present data are broadly consistent with the experimental results of the latter authors but imply systematically about 100°C higher temperatures, possibly because of the difference between the natural system and the simplified CaO-MgO-SiO_2 system adopted in the experimental procedure. The samples PHN-1611 and C 80-335 also show an enrichment of Ti and to a lesser extent Co. The four remaining olivine samples display an increase of Ca and Ti and a decrease of Cr and Zn with the increase of the Fo content.

Orthopyroxenes have a wide range of major- and trace-element contents. There is a broad positive correlation among Ti, Co, and the ratio 100Ca/(Ca + Mg) (Table 5) and among V, Mn, and Al. In addition, Ti and Mn are negatively correlated with the ratio 100Mg/(Mg + Fe) except in sample PHN-1611. The significant features of the trace-element variations in orthopyroxene are the relative depletion of V in the two garnet peridotites and the Ca, Ti, and Co enrichment in the two high-T xenoliths (PHN-1611 and C 80-335). A distinct depletion of Ti found in pyroxene PHN-1569 is probably due to the refractory character of the host rocks.

Clinopyroxenes display variations similar to the orthopyroxenes, but they also show a broad correlation between their major- and trace-element contents. In addition, clinopyroxene PHN-1611 is marked by a high concentration of Ni and Zn and a depletion of V (Table 6).

2. Variations of individual minerals within a single xenolith

The variation of Cr among pyroxene grains as described by Boyd and Finger (1975) in garnet peridotites is illustrated by the orthopyroxene of garnet-bearing sample PHN-1611 (Table 5). A similar Cr variation among the pyroxene grains is also observed in some spinel peridotites. For example, in sample MAN 91-1, the Cr content varies between 4500 and 5200 ppm in clinopyroxene and between 1950 and 2300 ppm in orthopyroxene (Fig. 1). However, the corresponding Cr partition coefficient between two adjacent pyroxenes remains constant, suggesting that domainal equilibrium was achieved. Some

TABLE 4. Ca and transition-element abundances (ppm) in olivine

		PHN-1569			C 80-335			MAN 91-1		
	PHN-1611	C	R(OPX)	R(CPX)	C	R(OPX)	R(CPX)	C	R(OPX)	R(CPX)
N:	10	12	3	3	17	4	5	12	2	4
Ca	1533	594	742	751	1601	1693	1631	1002	1021	1577
	(187)	(101)	(189)	(166)	(87)	(151)	(402)	(69)	(101)	(106)
Ti	175	<6	29	46	81	81	107	17	<6	20
	(28)		(25)	(41)	(24)	(37)	(13)	(9)		(8)
Cr	230	112	239	279	249	258	276	38	83	76
	(29)	(19)	(100)	(25)	(21)	(31)	(11)	(7)	(4)	(22)
Mn	962	747	753	779	1204	1212	1213	1064	1072	1049
	(10)	(15)	(9)	(20)	(44)	(21)	(18)	(12)	(22)	(41)
Co	157	124	124	119	145	158	158	139	134	131
	(12)	(18)	(9)	(10)	(14)	(10)	(10)	(13)	(18)	(7)
Ni	3047	3222	3191	3237	2533	2510	2528	2990	2960	2878
	(20)	(111)	(78)	(113)	(50)	(30)	(97)	(43)	(17)	(71)
Zn	110	64	52	63	71	69	66	49	48	54
	(9)	(11)	(2)	(8)	(7)	(9)	(10)	(12)	(1)	(15)
Fo (%)	88.5	92.9	93.0	93.0	89.3	89.3	89.3	90.5	90.5	90.5

Note: C—average contents of crystal cores; R(OPX), R(CPX), and R(SP)—average contents of rims at the contact with orthopyroxene, clinopyroxene, and spinel, respectively. OL"—secondary olivine in sample CAM-2B produced by the reaction diopside + Al-spinel → plagioclase + olivine + Cr-spinel. *N*—number of determinations. Values in brackets—standard deviation (1). Fo—forsterite content; olivine in sample PHN-1611 has homogeneous composition.

* Cr measured after masking the adjacent spinel grain with a thin W sheet.

other trace elements also show a small but distinct difference according to grain (e.g., in olivine PHN-1569, Ni = 3100 to 3350 ppm).

3. Variations of individual minerals within a single crystal (core to rim)

The olivine crystals of the high-T peridotites (PHN-1611 and C 80-335) have constant element composition within the limits of analytical error, but the olivines of the low-T peridotites (PHN-1569, MAN 91-1, LEZ-1, and CAM-2B) display changes in composition at the outer rim, not exceeding 100 μm in width. The variation is particularly apparent for Ca and Cr, which have lower concentrations in the olivine cores of the low-T peridotites than in those of the high-T peridotites: in the outer rim of the low-T peridotites, the Ca and Cr concentrations are equivalent to those in the unzoned olivines of the high-T peridotites (Table 4). The enrichment of these elements in the olivine rims depends also on the mineral in contact with olivine; in sample LEZ-1, for example, the contact rim with clinopyroxene is higher in Ca but lower in Cr than the contact with spinel (Table 4). In addition, Ni decreases slightly at the outer rims of olivine in the low-T spinel-plagioclase peridotite (CAM-2B). These features indicate disequilibrium at the grain margins and may be related to a heating event of short duration (Takahashi, 1980).

In both ortho- and clinopyroxene, the differences in trace-element characteristics between core and rim and the proportions of mineral grains with a constant concentration are different for different elements (Figs. 1 and 2) and are highly variable among the samples. This may reflect the complexity and variability of the processes associated with the xenolith genesis. Mn, Ni, and V remain constant between core and rim in some samples, but in

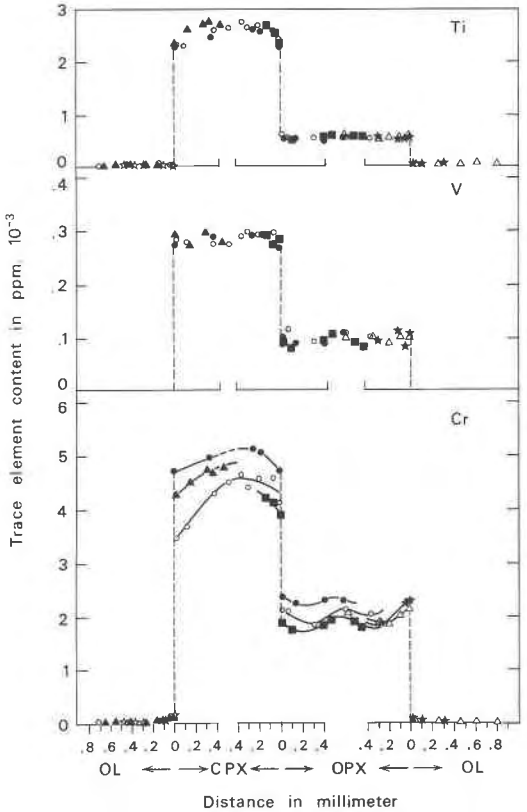

Fig. 1. Ti, V, and Cr contents of mineral phases of sample MAN 91-1 plotted against the distance from the grain boundaries. Each symbol represents different mineral grain. OL = olivine, OPX = orthopyroxene, CPX = clinopyroxene.

TABLE 4—*Continued*

LEZ-1				CAM-2B			
C	R(OPX)	R(CPX)	R(SP)	C	R(OPX)	R(CPX)	OL"
15	3	3	1	11	4	4	2
942	1157	1880	1521	1015	1082	1449	2065
(97)	(260)	(334)		(133)	(156)	(163)	(172)
12	<6	30	10	20	16	26	95
(14)		(26)		(17)	(13)	(20)	(24)
63	129	155	538*	21	75	113	346
(14)	(55)	(14)		(11)	(57)	(21)	(1)
1011	1008	1005	1063	1149	1156	1145	1201
(19)	(13)	(24)		(15)	(37)	(13)	(1)
126	136	130	112	128	121	113	125
(12)	(11)	(8)		(16)	(3)	(11)	(8)
2936	2909	2822	2813	2762	2660	2665	2364
(73)	(60)	(65)		(60)	(178)	(147)	(41)
52	54	60	95	42	52	47	46
(10)	(8)	(3)		(11)	(13)	(15)	(4)
90.8	90.8	90.8	90.3	89.3	89.5	89.5	89.6

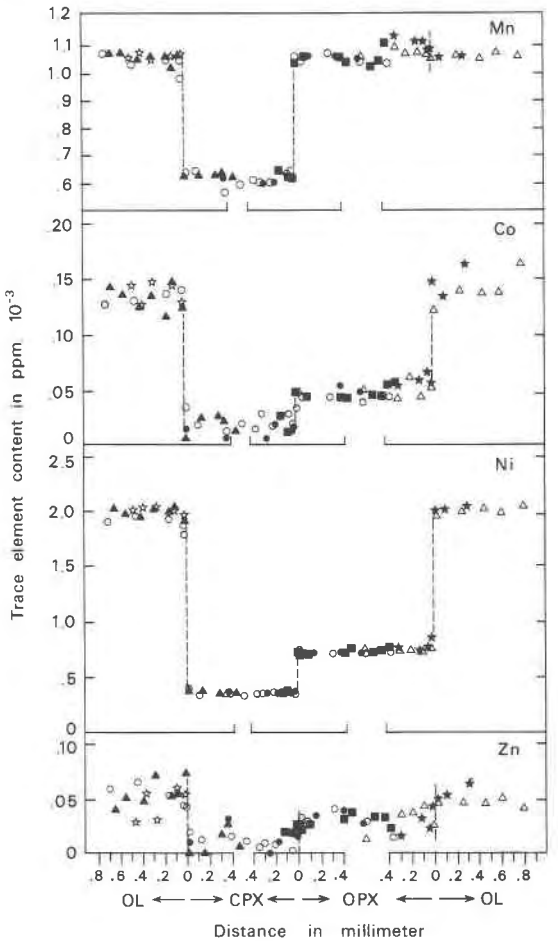

Fig. 2. Mn, Co, Ni, and Zn contents of mineral phases of sample MAN 91-1 plotted against the distance from the grain boundaries. Each symbol represents different mineral grain.

others, Ni and Mn increase slightly at the rim. The most significant increase of Ni is observed in the spinel-plagioclase lherzolite (Ni = 250 ppm in the core and 350 ppm in the rim of the clinopyroxene, Table 6). On the other hand, its distribution is rather homogeneous in the high-T and high-P xenoliths, particularly in garnet lherzolite PHN-1611.

Cr has the largest range of variations and shows at least three types of distribution patterns (Figs. 1 and 3). In the pyroxenes of samples CAM-2B and the clinopyroxene of sample MAN 91-1, Cr displays a bell-shaped pattern showing a distinct decrease toward the rim and is strongly correlated with Ti and Al. Conversely, Cr increases toward the rim in the pyroxenes from garnet peridotite PHN-1569 and also in the orthopyroxenes of sample C 80-335. In other cases, only a slight decrease of Cr toward the rim is noted. The analytical precision for Zn and Co is not sufficient to detect any significant variation between the core and the rim of the pyroxenes.

The garnet grains were analyzed only in sample PHN-1611. V, Co, Ni, and Zn are homogeneously distributed within the limits of experimental error. On the other hand, Ti increases steadily from the core to the rim, and Cr is depleted at the rim. A similar inverse distribution of Ti and Cr has been reported for garnet of peridotite xenoliths by Smith and Ehrenberg (1984) and Smith and Boyd (1984) for PHN-1611. The latter authors partly attributed the zonation to crystal growth during metasomatism.

Partition coefficients

Compositional zoning in minerals is usually interpreted to be the result of a disequilibrium process due to (1) primary growth crystallization from a liquid or subsolidus crystallization, (2) resorption of grain margins during

Table 5. Ca and transition-element abundances (ppm) in orthopyroxene

	PHN-1611			PHN-1569			C 80-335		
	(1)	(2)	(3)	C	R(OL)	R(CPX)	C	R(OL)	R(CPX)
N:	6	9	6	11	3	3	2	4	2
Ca	12493	12917	12811	3030	2995	3321	8859	10713	10416
	(125)	(250)	(698)	(165)	(151)	(176)	(506)	(221)	(286)
Ti	1380	1342	1334	35	49	55	1605	1932	1922
	(51)	(74)	(152)	(22)	(37)	(14)	(239)	(54)	(54)
V	60	62	57	31	45	52	115	95	162
	(9)	(14)	(17)	(16)	(15)	(14)	(21)	(29)	(62)
Cr	1278	937	1439	2299	2634	2754	3627	4182	4209
	(31)	(25)	(41)	(81)	(25)	(28)	(53)	(96)	(80)
Mn	986	986	1012	868	878	843	1150	1160	1162
	(15)	(12)	(17)	(23)	(3)	(42)	(16)	(11)	(40)
Co	82	87	82	45	44	43	74	70	92
	(4)	(6)	(5)	(7)	(9)	(1)	(3)	(9)	(3)
Ni	1016	999	1055	770	813	801	741	745	728
	(15)	(14)	(19)	(21)	(7)	(6)	(7)	(15)	(6)
Zn	62	71	65	31	39	39	42	48	38
	(15)	(11)	(15)	(16)	(30)	(15)	(25)	(10)	(4)
Al_2O_3 (%)	1.49	1.52	1.48	0.99	1.06	1.10	5.70	6.39	6.36
100Ca/(Ca + Mg)	3.3	3.4	3.4	0.8	0.8	0.9	2.7	3.3	3.2
100Mg/(Mg + Fe)	89.3	89.4	89.4	93.8	93.7	93.7	89.6	89.5	89.5

Note: C—average contents of the core; R(OL), R(CPX), and R(SP)—average contents of the rims at the contact with olivine, clinopyroxene, and spinel, respectively. Orthopyroxene in sample PHN-1611 is homogeneous within a single crystal but displays differences among the crystals; thus three analyzed grains are reported separately. *N*—number of determinations.

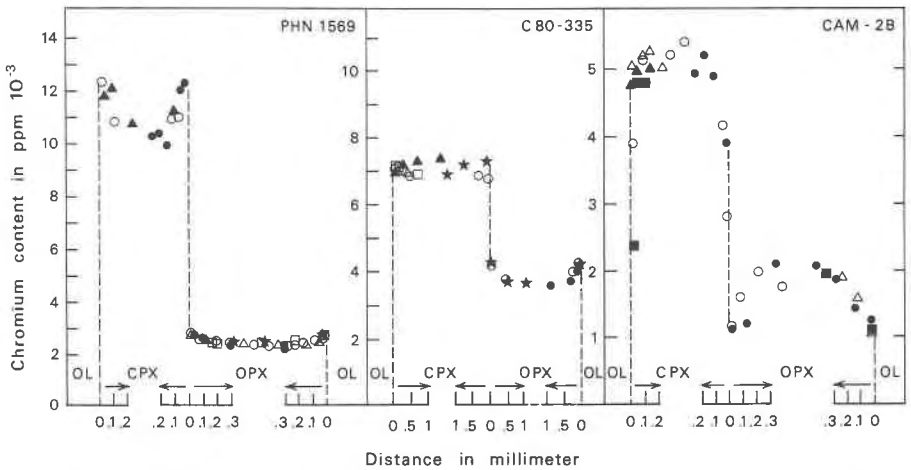

Fig. 3. Cr contents in clino- and orthopyroxene of samples PHN-1569, C 80-335, and CAM-2B plotted against the distance from the crystal boundaries. Each symbol represents different mineral grain.

partial melting, or (3) diffusional cation exchange between minerals. Although our data are not sufficient to decipher the factors involved in the origin of the zoning, they can be used to put some constraints on the process.

In the analyzed samples, the changes in abundances of Ca, Cr, and Ni toward the rim of the olivine are clearly related to the composition of the adjacent mineral, thus favoring a diffusional cation-exchange process. However, the volume over which such a process may have acted is limited to the outermost part of the crystal, and the data indicate that at least three-quarters of the volume of olivine were not affected by this process. A similar process can also be invoked for pyroxenes of the low-T peridotites that show, for example, a slight but distinct increase of Ni in the rim adjacent to olivine.

On the other hand, the zoning pattern of Cr in pyroxenes is more variable and involves a larger proportion of the crystal than any other analyzed element. The largest Cr and Ti variations in pyroxenes are found in spinel-plagioclase lherzolite CAM-2B (Tables 5 and 6). In Figure 3, Cr is shown to decrease from the core to the rim in both the ortho- and clinopyroxene. In fact, these minerals are also strongly zoned for major elements (Dautria and Girod, 1986), and Cr correlates positively with Al. The variation of the latter element is consistent with a re-equilibration process related to the adiabatic uplift up to the boundary between spinel and plagioclase facies (e.g., Gasparik, 1984). The decrease of Cr and Al toward the rim in both ortho- and clinopyroxene suggests the operation of an intergranular cation-exchange process with

TABLE 5—*Continued*

MAN 91-1				LEZ-1			CAM-2B		
C	R(OL)	R(CPX)	R(SP)	C	R(OL)	R(CPX)	C	R(OL)	R(CPX)
9	2	3	2	6	3	3	6	3	2
4964	5738	6048	5473	4323	4639	5022	4220	4346	4960
(194)	(33)	(25)	(147)	(118)	(231)	(478)	(177)	(210)	(113)
556	562	553	569	286	264	298	901	520	487
(38)	(24)	(40)	(66)	(32)	(37)	(24)	(112)	(14)	(1)
99	102	95	111	74	70	78	86	74	65
(10)	(2)	(6)	(1)	(24)	(20)	(25)	(15)	(3)	(4)
2061	2242	2144	2819	2766	2667	2682	2062	1130	1128
(177)	(103)	(235)	(16)	(40)	(105)	(51)	(186)	(116)	(28)
1050	1076	1052	1094	1067	1048	1040	1183	1204	1185
(12)	(6)	(9)	(4)	(14)	(24)	(29)	(18)	(9)	(41)
47	54	42	52	40	45	44	37	29	43
(5)	(2)	(7)	(2)	(6)	(7)	(11)	(12)	(2)	(20)
721	806	723	770	698	716	698	583	660	628
(20)	(61)	(10)	(17)	(16)	(28)	(10)	(33)	(25)	(41)
28	35	27	51	37	30	40	14	36	20
(9)	(12)	(6)	(9)	(17)	(13)	(14)	(13)	(18)	(3)
4.25	4.47	4.41	4.57	2.75	2.75	2.75	4.82	3.33	3.29
1.4	1.6	1.7	1.5	1.2	1.3	1.4	1.1	1.1	1.3
90.7	90.7	90.7	90.7	91.6	91.5	91.5	89.7	89.9	89.9

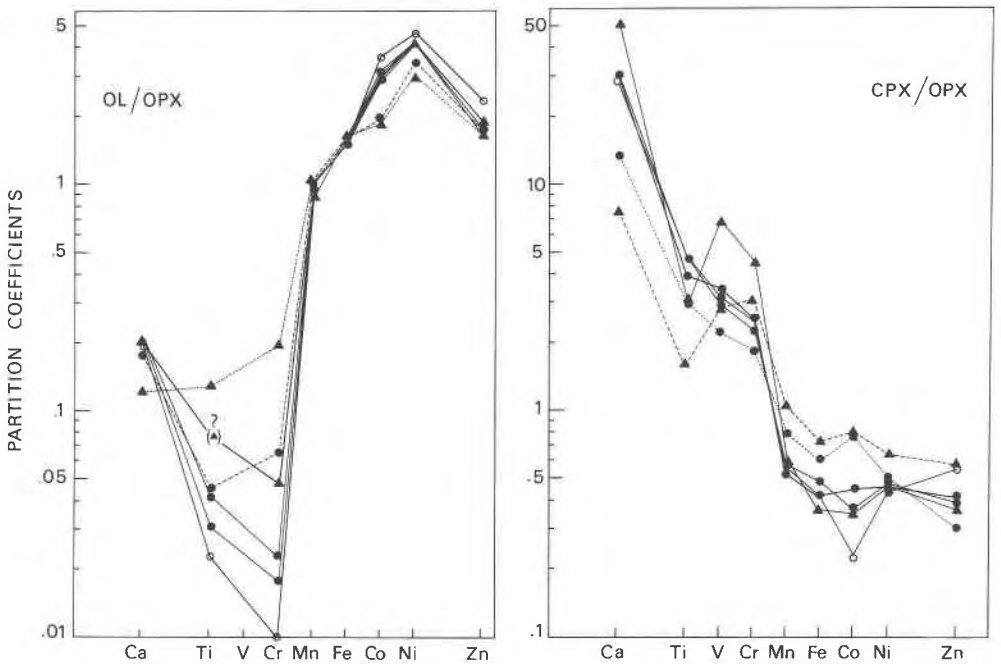

Fig. 4. Partition coefficients calculated using the average trace-element contents of the core of minerals. Garnet peridotite, triangles; spinel peridotites, solid circles; spinel-plagioclase peridotite, empty circles. The solid lines represent low-T peridotites (PHN-1569, MAN 91-1, LEZ-1, and CAM-2B), whereas the dashed lines correspond to high-T peridotites (PHN-1611 and C 80-335). $K_{Ti}^{Ol/Opx}$ in sample PHN-1569 was calculated assuming Ti = 3 ppm in olivine.

spinel by means of grain-boundary diffusion. This process is also consistent with the symmetrical zoning observed in orthopyroxene, which has the same rim composition whether the the mineral in contact is clinopyroxene or olivine (Fig. 3 and Table 5). The efficiency of grain-boundary diffusion, for which there is evidence in sample CAM-2B, is compatible with the development of a network of silicate melts during mantle upwelling (cf. McKenzie, 1985).

The regular and symmetrical zoning observed in both ortho- and clinopyroxene is similar to that registered in high-temperature alpine peridotites (e.g., Obata, 1980). Clinopyroxene adjacent to spinel displays a superimposed asymmetrical zoning marked by the presence of cloudy, Al-Na–depleted domains resembling the turbid clinopyroxene borders described by Carswell (1975). They have been related to a late melting event, synchronous with the plagioclase-forming reaction (Dautria and Girod, 1986).

On the other hand, Cr in ortho- and clinopyroxene may display a U-shaped zoning pattern (garnet harzburgite PHN-1569), which is probably not the result of diffusional re-equilibration since the pyroxenes have very homogeneous contents of major elements (Boyd and Finger, 1975) and Cr is not correlated with Al in this sample. Growth crystallization would probably not cause such patterns since the partition coefficients of Cr between pyroxenes and either a melt or a solid peridotite matrix would be higher than 1, at least for clinopyroxene. On the other hand, the resorption of pyroxene crystals during partial melting, accompanied by a bulk diffusion of Cr within the grains, can account for the observed U-shaped patterns. In fact, partial melting of the grain boundaries would probably concentrate Cr at the pyroxene rims if the diffusional flow of this element toward the core was relatively slow compared to the crystal resorption rate. Thus it is suggested that equilibrium between solid and liquid may be achieved depending on the diffusional rates of the different elements in the residual minerals. In our samples, only Cr displays significant evidence of disequilibrium melting.

None of the other Cr zoning patterns can be explained by one process alone. For example, the compositional zoning of pyroxenes in sample MAN 91-1 (Fig. 1) suggests that both diffusional cation exchange between adjacent minerals and grain-boundary diffusion have superimposed their effects on the bell-shaped profiles formed during a previous event. All these considerations indicate the complexity and variability of the processes that have affected the chemical composition of the minerals in the different samples. Except for Cr and Ti, the constancy of the other elements in most of the crystals suggests that equilibrium conditions were confined to the core of the minerals. In the following section, partition coefficients of transition elements between various mineral pairs are discussed.

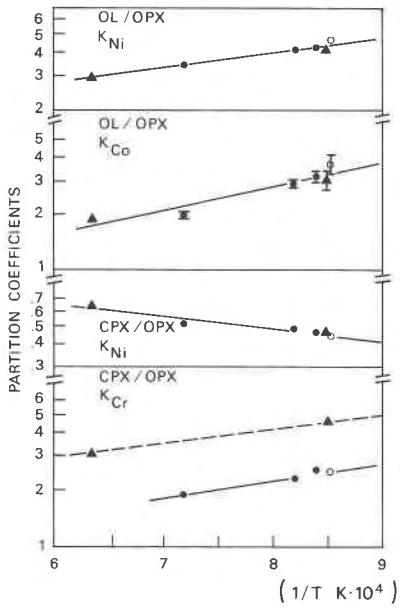

Fig. 5. Van't Hoff plot of partition coefficients vs. T taken from Table 1 (geothermometer of Wells, 1977).

Olivine-orthopyroxene

The Nernst partition coefficients between olivine and orthopyroxene ($K_D^{Ol/Opx}$) display approximately the same patterns in the different peridotites (Fig. 4). This pattern is characterized by K_D values of >1 for Co, Ni, and Zn, ~ 1 for Mn, and <1 for Ca, Cr, and Ti. The K_D values are in the range of those reported by Stosch (1981) and Hervig and Smith (1982). In the studied samples, the observed variations are related to T and/or P conditions of equilibration. The $K_D^{Ol/Opx}$ for the bivalent elements Ni, Co, Mn, and Ca is mainly controlled by temperature as shown from the Van't Hoff plot (Fig. 5). This graph indicates that $K_{Ni}^{Ol/Opx}$ and $K_{Co}^{Ol/Opx}$ increase regularly with decrease of temperature. The tri- and tetravalent elements behave differently and appear to have a more complex variation. The variation of the $K_{Cr}^{Ol/Opx}$ (Fig. 5) implies the influence of both P and T as suggested by Hervig and Smith (1982): the highest $K_{Cr}^{Ol/Opx}$ (0.2) is encountered in the high-P, high-T sample PHN-1611, and the lowest value (0.01) is found in the low-P, low-T spinel-plagioclase peridotite CAM-2B. Among the other samples, both the high-T spinel peridotite C 80-335 and the low-T garnet peridotite PHN-1569 display higher values (0.044–0.066) than the low-P, low-T spinel lherzolites LEZ-1 and MAN 91-1 (0.019–0.023). This suggests that the $K_{Cr}^{Ol/Opx}$ increases with both T and P. $K_{Ti}^{Ol/Opx}$ should be also influenced by T and P, but the rather good correlation with P (Fig. 6) suggests a predominant effect of P. However, the number of other factors that may influence the partition of trace transition elements between minerals (e.g., compositional effects—Bishop et al., 1978) prevent us from generalizing at this stage.

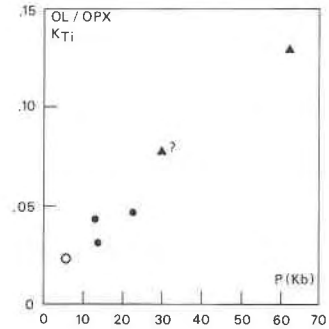

Fig. 6. Partition coefficients of Ti between olivine and orthopyroxene plotted against P taken from Table 1.

Clinopyroxene-orthopyroxene

The partition coefficients between clino- and orthopyroxene ($K_D^{Cpx/Opx}$) decrease from Ca to Zn (Fig. 4). The patterns for garnet peridotite differ from those of spinel peridotite by higher $K_V^{Cpx/Opx}$ and $K_{Cr}^{Cpx/Opx}$ but lower $K_{Ti}^{Cpx/Opx}$ values. The shape of the patterns and the $K_D^{Cpx/Opx}$ values are closely comparable to those found in peridotites of equivalent mineralogical composition (Liotard and Dupuy, 1980). As in the orthopyroxene-olivine pairs, the $K_D^{Cpx/Opx}$ variations suggest a temperature dependence for the bivalent elements Mn, Co, and Ni (Fig. 5) with the highest values in the high-T peridotites. The complex variations of the tri- and tetravalent elements Ti, V, and Cr reflect the influence of T, P, and possibly variable redox states among the nodules. The lowest $K_{Ti}^{Cpx/Opx}$ values are encountered in the high-P, high-T sample PHN-1611, and the highest values are found in the low-P, low-T spinel-plagioclase sample CAM-2B. This suggests that the $K_{Ti}^{Cpx/Opx}$ value decreases with both T and P. On the other hand, the lowest values of $K_V^{Cpx/Opx}$ and $K_{Cr}^{Cpx/Opx}$ are found in the high-T spinel peridotite C 80-335, the highest values are in the low-T garnet peridotite PHN-1569, and both the high-P, high-T garnet peridotite PHN-1611 and the low-P, low-T spinel-plagioclase peridotite CAM-2B have intermediate values. This might indicate that the $K_D^{Cpx/Opx}$ values for V and Cr increase with T and decrease with P.

Clinopyroxene-garnet

The partition coefficients involving garnet are only available for sample PHN-1611. The $K_D^{Cpx/Gt}$ value (Fig. 7) shows that Ni and Zn in addition to Ca are preferentially incorporated into the clinopyroxene. The other transition elements are more enriched in garnet, with the exception of Co that has approximately the same content in the two minerals. The published partition coefficients for the same mineral pairs from ultramafic rocks (Dupuy et al., 1980) are also reported in Figure 7, indicating a large range of K_D values for most transition elements with variations dependent upon P-T conditions of equilibration. For example, $K_V^{Cpx/Gt}$ is greater than one (2.5–3.0) at approximately 20 kbar whereas it is 0.68 at 63 kbar, rein-

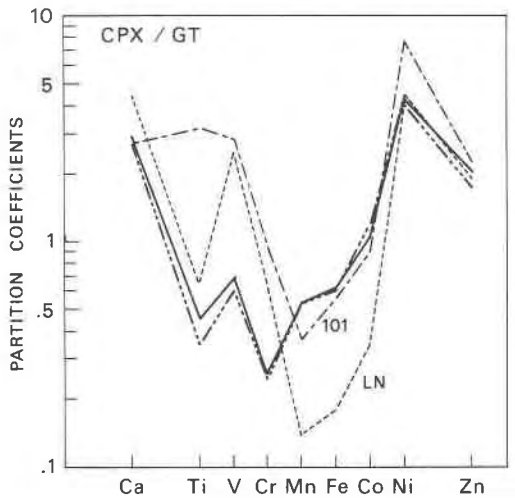

Fig. 7. Clinopyroxene-garnet partition coefficients for sample PHN-1611 calculated using the average contents of the core (solid line) and rim (thick dashed line) of the crystals. Data of Dupuy et al. (1980) for samples LN and 101 are also shown for comparison. Equilibrium conditions for LN, 18 kbar and 780°C; those for 101, 20 kbar and 1200°C.

forcing the suggestion of Shimizu and Allègre (1978) that this partition coefficient could be a very good geobarometer.

$K_{Cr}^{Cpx/Gt}$ also decreases with P (from 0.6 to 1.0 at about 20 kbar to 0.25 at 63 kbar) but possibly increases with T. $K_{Mn}^{Cpx/Gt}$ correlates only with T: this parameter increases from 0.14 in the sample equilibrated at 780°C, to 0.37 in the one equilibrated at 1200°C and finally to 0.53 at 1300–1400°C (PHN-1611). $K_D^{Cpx/Gt}$ for Ti, Co, and Ni shows more complex variations, and the available data are consistent with a positive dependence on T and a negative one on P.

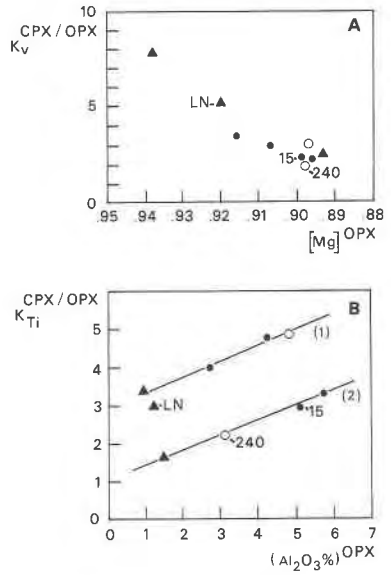

Fig. 8. (A) Partition coefficient of V between clinopyroxene and orthopyroxene plotted against 100Mg/(Mg + Fe) of orthopyroxene (= $[Mg]^{OPX}$). The symbols are the same as in Fig. 4. (B) Partition coefficient of Ti between clinopyroxene and orthopyroxene plotted against the Al_2O_3 content of orthopyroxene; (1) a regression line for low-T peridotites (T < 1000°C), (2) a line connecting the two high-T peridotites (T > 1100°C). Three samples of Liotard and Dupuy (1980) are shown for a comparison: LN, a garnet pyroxenite (equilibrium T = 780°C); 15, a spinel peridotite (T = 1160°C); 240, a plagioclase peridotite (T = 1160°C).

Effects of composition on K_D values

The K_D variation for the studied mineral pairs not only correlates with T and P but also with the major-element composition of the phases. The influence of this param-

TABLE 6. Transition-element abundances (ppm) in clinopyroxene

	PHN-1611		PHN-1569			C 80-335		
	C	R(OL)	C	R(OL)	R(OPX)	C	R(OL)	R(OPX)
N:	9	8	6	3	3	10	5	2
Ti	2228	2176	120	132	141	5248	5553	5338
	(58)	(62)	(36)	(15)	(30)	(710)	(173)	(54)
V	154	150	236	250	218	242	249	254
	(10)	(10)	(10)	(12)	(13)	(23)	(36)	(8)
Cr	3851	3503	10345	12091	12263	7075	7092	7055
	(110)	(63)	(292)	(278)	(60)	(207)	(50)	(356)
Mn	1038	1063	527	491	525	919	945	936
	(16)	(11)	(11)	(12)	(24)	(19)	(28)	(6)
Co	64	67	16	15	17	58	62	55
	(7)	(3)	(9)	(14)	(12)	(9)	(7)	(4)
Ni	661	664	371	363	380	377	394	379
	(12)	(17)	(12)	(11)	(0)	(12)	(22)	(15)
Zn	41	33	9	16	12	16	7	18
	(14)	(13)	(12)	(9)	(10)	(11)	(5)	(5)
Al_2O_3 (%)	2.67	2.68	2.11	2.18	2.19	7.73	8.10	8.15
100Ca/(Ca + Mg)	31.8	31.6	47.9	47.9	47.9	44.2	43.6	43.6
100Mg/(Mg+ Fe)	88.0	88.0	95.0	95.0	95.0	87.9	87.8	87.8

Note: Abbreviations are the same as in Table 4.

eter is shown in Figures 8A and 8B. Figure 8A indicates that $K_V^{Cpx/Opx}$ decreases regularly with the 100Mg/(Mg + Fe) ratio in the orthopyroxene. In Figure 8B, $K_{Ti}^{Cpx/Opx}$ is separated into two groups that differ in temperature of equilibration. Within each group, $K_{Ti}^{Cpx/Opx}$ increases sympathetically with Al_2O_3 in the orthopyroxene. It is of interest that published data on $K_{Ti}^{Cpx/Opx}$ (Liotard and Dupuy, 1980) display the same variations as our samples (Fig. 8B).

K_D calculated from the rims

In the previous discussion, the partition coefficients were based upon the composition of the mineral cores. However, there are some differences in the K_D values calculated from the rim of two adjacent minerals, and such values may provide complementary petrogenetic information.

For the high-T peridotites, there is either no difference in K_D values obtained from the rim and core (e.g., sample PHN-1611), or their variation is related to an increased T of exchange toward the rim (e.g., sample C 80-335). This observation also applies to divalent ions such as Ni in the low-T peridotites. However, the scatter of the K_D values for Ca, Ti, and Cr obtained on the rim of the grains in the low-T peridotites suggests nonequilibrium conditions, which could be due to slower solid diffusion rates for these elements. For example, the interdiffusion rate of Ca in olivine crystals (Takahashi, 1980; Morioka, 1981) is notably smaller than that of Fe-Mg, supporting the contention that there was probably insufficient time for low-T peridotites to reach equilibrium.

Discussion

The electron microprobe can provide high-quality data on the abundances of minor and trace transition elements in silicates of ultramafic rocks. The method can be used to evaluate whether chemical equilibration among minerals was disturbed by postcrystallization thermal events that frequently affect ultramafic xenoliths. Overall, the analyses show that the interiors of the grains are rather homogeneous for the analyzed elements except Cr and to a lesser extent Ti and Ca in pyroxenes. In olivine, a concentration gradient appears only in the outermost part of the crystal and is probably related to a late thermal event.

The partition coefficients obtained in this study can be used in geochemical modeling provided that P, T, and mineral composition are considered. The K_D values are affected by these factors, and their influence is variable for different elements. For example, K_{Ni} is mainly influenced by T, whereas K_D values for Ca, Ti, Cr, and V display a correlation with P and/or composition of the phase. For some elements, these parameters may act in an inverse manner. For the clinopyroxene-orthopyroxene pair, K_{Cr} and K_V increase but K_{Ti} decreases with increasing P. This implies a change of sign for the molar volume of the exchange reaction and may reflect variable substitu-

TABLE 7. Transition-element abundances (ppm) in garnet from sample PHN-1611

	Zoned*		
	C	R(OL)	Unzoned†
N:	3	2	6
Ti	4881 (67)	6430 (74)	6281 (15)
V	229 (15)	240 (21)	265 (7)
Cr	14259 (177)	13563 (735)	15024 (123)
Mn	1987 (36)	1991 (32)	1986 (2)
Co	65 (1)	56 (1)	69 (14)
Ni	155 (7)	167 (8)	160 (12)
Zn	18 (4)	23 (1)	28 (17)

Note: Abbreviations are the same as in Table 4.
* Large zoned section (~3 mm in diameter).
† Small unzoned section (~0.3 mm in diameter).

TABLE 6—*Continued*

MAN 91-1			LEZ-1			CAM-2B		
C	R(OL)	R(OPX)	C	R(OL)	R(OPX)	C	R(OL)	R(OPX)
10	3	3	12	3	3	7	4	3
2611	2290	2314	1118	1027	1089	4253	(4397–3291)	(3259–2436)
(82)	(40)	(70)	(48)	(54)	(9)	(177)		
291	283	274	245	262	252	265	291	267
(13)	(8)	(8)	(15)	(9)	(11)	(14)	(22)	(19)
4744	4161	4236	6968	6634	6608	5162	(5067–2397)	(4168–2820)
(237)	(623)	(420)	(542)	(47)	(210)	(172)		
616	643	639	568	623	616	679	637	671
(14)	(5)	(13)	(27)	(19)	(42)	(23)	(18)	(24)
18	19	16	18	29	24	8	9	8
(7)	(15)	(3)	(10)	(13)	(6)	(7)	(10)	(13)
348	384	351	320	349	330	253	315	356
(11)	(7)	(4)	(14)	(12)	(11)	(27)	(26)	(82)
12	9	20	12	4	15	20	14	9
(10)	(10)	(6)	(12)	(4)	(18)	(11)	(10)	(8)
5.90	5.70	5.64	3.70	3.91	3.94	7.98	7.70–5.55	6.53–5.36
49.9	49.8	49.8	48.5	47.6	47.6	50.5	49.7	49.7
90.4	90.1	90.1	92.6	92.1	92.1	90.0	90.6	90.6

tion sites for the transition elements. Cr^{3+} and V^{3+} display a strong preference for octahedral sites (Burns, 1970). On the other hand, Ti^{4+}, which has no significant ligand-field stabilization energy, may be shared between octahedral and tetrahedral sites (Sack and Carmichael, 1984).

The partitioning of trace transition elements among the coexisting phases of ultramafic rocks may yield good geothermometers and geobarometers once experimental calibration has been done. Because of their high sensitivity to physical parameters, some of these trace elements can also provide information concerning the petrogenetic history of ultramafic rocks. Among the analyzed trace transition elements, Cr appears to have the lowest diffusional rate in the residual minerals and best demonstrates evidence of disequilibrium melting.

Acknowledgments

This paper has been greatly improved by the review of D. Smith and another anonymous referee, and through discussion with A. Baronnet. Thanks are also due to J. C. Mercier, J. Fabriès, M. Girod, J. M. Dautria, and J. P. Lorand for providing the samples. This study was financially supported by the A.T.P. "Distribution des éléments à l'échelle cristalline et fractionnements géochimiques" of the CNRS, France.

References

Adams, G.E., and Bishop, F.C. (1982) Experimental investigation of Ca-Mg exchange between olivine, orthopyroxene and clinopyroxene: Potential for geobarometry. Earth and Planetary Science Letters, 57, 241–250.

Ancey, M., Bastenaire, F., and Tixier, R. (1978) Applications des méthodes statistiques en micro-analyse. In Micro-analyse et microscopie électronique à balayage, 322–344. Les Editions de Physique, Orsay, France.

Armigliato, A., Dori, L., Garulli, A., and Venturi, P. (1982) X-ray microanalysis of nitrogen in presence of titanium with an automated microprobe. Journal de Microscopie et de Spectroscopie électroniques, 7, 593–603.

Bence, A.E., Brande, S., Indelicato, G.J., and Allen, F. (1980) Analysis of trace and minor elements in rock forming minerals using an automated electron probe. In D.R. Beaman, R.E. Ogilvie, and D.B. Wittry, Eds., 8th International Congress on X-Ray Optics and Microanalysis, p. 538–548, Pendell Publishing Company, Midland, Michigan.

Berger, E.T. (1981) Enclaves ultramafiques, mégacristaux et leurs basaltes-hôtes en contexte océanique (Pacifique sud) et continental (Massif Central français). Thèse d'Etat, Paris, 470 p.

Bertrand, P., and Mercier, J. C. (1986) The mutual solubility of coexisting ortho- and clinopyroxene: Toward an absolute geothermometer for the natural system. Earth and Planetary Science Letters, 76, 109–112.

Bishop, F. C., Smith, J. V., and Dawson, J. B. (1978) Na, K, P and Ti in garnet, pyroxene and olivine from peridotite and eclogite xenoliths from African kimberlites. Lithos, 11, 155–173.

Bizouard, H. (1982) L'analyse par microsonde électronique des éléments en faible teneur dans les minéraux et verres naturels. Journal de Microscopie et de Spectroscopie électroniques, 7, 543–554.

Boyd, F.R., and Finger, L.W. (1975) Homogeneity of minerals in mantle rocks from Lesotho. Carnegie Institution of Washington Year Book 74, 519–525.

Burns, R.G. (1970) Mineralogical applications of crystal field theory. Cambridge University Press, Cambridge, 224 p.

Carswell, D.A. (1975) Primary and secondary phlogopites and clinopyroxenes in garnet lherzolite xenoliths. Physics and Chemistry of the Earth, 9, 417–429.

Coisy, P. (1977) Structure et chimisme des péridotites en enclaves dans les basaltes du Massif Central—Modèles géodynamiques du manteau supérieur. Thèse, troisième cycle, Nantes, 115 p.

Dautria, J.M., and Girod, M. (1986) Les enclaves de lherzolite à spinelle et plagioclase du volcan de Dibi (Adamaoua, Cameroun): Des témoins du manteau supérieur anormal. Bulletin de Minéralogie, 109, 275–288.

Delaney, J.S., Smith, J.V., Dawson, J.B., and Nixon, P.H. (1979) Manganese thermometer for mantle peridotite. Contributions to Mineralogy and Petrology, 71, 157–170.

Delano, J.W. (1986) Pristine lunar glasses: Criteria, data and implications. Journal of Geophysical Research, 91, D201–D213.

Dupuy, C., Dostal, J., Liotard, J.M., and Leyreloup, A. (1980) Partitioning of transition elements between clinopyroxene and garnet. Earth and Planetary Science Letters, 48, 301–310.

Fabriès, J. (1979) Spinel-olivine geothermometry in peridotites from ultramafic complexes. Contributions to Mineralogy and Petrology, 69, 329–336.

Finnerty, A.A., and Boyd, F.R. (1978) Pressure-dependent solubility of calcium in forsterite coexisting with diopside and enstatite. Carnegie Institution of Washington Year Book 77, 713–717.

Gasparik, T. (1984) Two-pyroxene thermobarometry with new experimental data in the system CaO-MgO-Al_2O_3-SiO_2. Contributions to Mineralogy and Petrology, 87, 87–97.

Girod, M., Dautria, J.M., and de Giovanni, R. (1981) A first insight into the constitution of the upper mantle under the Hoggar area (southern Algeria): The lherzolite xenoliths in the alkali basalts. Contributions to Mineralogy and Petrology, 77, 66–73.

Hervig, R.L., and Smith, J.V. (1982) Temperature-dependent distribution of Cr between olivine and pyroxenes in lherzolite xenoliths. Contributions to Mineralogy and Petrology, 81, 184–189.

Hervig, R.L., Smith, J.V., Steele, I.M., and Dawson, J.B. (1980) Fertile and barren Al-Cr-spinel harzburgites from the upper mantle: Ion and electron probe analyses of trace elements in olivine and orthopyroxene: Relation to lherzolites. Earth and Planetary Science Letters, 50, 41–58.

Kushiro, I., Shimizu, N., and Nakamura, Y. (1972) Compositions of coexisting liquid and solid phases formed upon melting of natural garnet and spinel lherzolites at high pressure: A preliminary report. Earth and Planetary Science Letters, 14, 19–25.

Liotard, J.M., and Dupuy, C. (1980) Partage des éléments de transition entre clinopyroxene et orthopyroxene: Variations avec la nature des roches. Chemical Geology, 28, 307–309.

Lucazeau, F., and Bayer, R. (1982) Evolution géothermique et géodynamique du Massif Central français depuis l'Oligocène. Annales de Géophysique, 38, 405–429.

McKay, G.A. (1986) Crystal/liquid partitioning of REE in basaltic systems: Extreme fractionation of REE in olivine. Geochimica et Cosmochimica Acta, 50, 69–79.

McKenzie, D. (1985) The extraction of magma from the crust and mantle. Earth and Planetary Science Letters, 74, 81–91.

Mercier, J.C., and Carter, N.L. (1975) Pyroxene geotherms. Journal of Geophysical Research, 80, 3349–3362.

Morioka, M. (1981) Cation diffusion in olivine—II. Ni-Mg, Mn-Mg and Mg-Ca. Geochimica et Cosmochimica Acta, 45, 1573–1580.

Nicolas, A., Lucazeau, F., and Bayer, R. (1987) Peridotite xenoliths in Massif Central basalts: Textural and geophysical evidence for asthenosphere diapirism. In P.H. Nixon, Ed., Mantle xenoliths, p. 566–573. Wiley, London.

Nixon, P.H., and Boyd, F.R. (1973) Petrogenesis of the granular and sheared ultrabasic nodule suite in kimberlites. In P.H. Nixon, Ed., Lesotho kimberlites, p. 48–56. Lesotho National Development Corp., Maseru, Lesotho.

Obata, M. (1980) The Ronda peridotite: Garnet, spinel, and plagioclase lherzolite facies and the P-T trajectories of a high-temperature mantle intrusion. Journal of Petrology, 21, 533–572.

Sack, R.O., and Carmichael, I.S.E. (1984) $Fe^2 \rightleftharpoons Mg^2$ and $TiAl_2 \rightleftharpoons MgSi_2$ exchange reactions between clinopyroxenes and silicate melts. Contributions to Mineralogy and Petrology, 85, 103–115.

Shimizu, N. (1978) Analysis of a zoned plagioclase of different magmatic environments: A preliminary ion-microprobe study. Earth and Planetary Science Letters, 39, 398–406.

Shimizu, N., and Allègre, J.C. (1978) Geochemistry of transition elements in garnet lherzolite nodules in kimberlites. Contributions to Mineralogy and Petrology, 67, 41–50.

Smith, D., and Boyd, F.R. (1984) Mineral heterogeneities in high T lherzolite nodules. EOS, 65, 1154.

——— (1987) Compositional heterogeneities in a high-temperature lherzolite nodule and implications for mantle processes. In P.H. Nixon, Ed., Mantle xenoliths, Wiley, London, in press.

Smith, D., and Ehrenberg, S.N. (1984) Zoned minerals in garnet peridotite nodules from the Colorado plateau; implications for mantle metasomatism and kinetics. Contributions to Mineralogy and Petrology, 86, 274–285.

Sotin, C., Bertrand, P., and Mercier, J.C. (1987) Physical and chemical properties of the upper mantle beneath Precambian shields. Physics of Earth and Planetary Interiors, in press.

Statham, P.J. (1977) Deconvolution and background subtraction by least-squares fitting with prefiltering of spectra. Analytical Chemistry, 49, 2149–2154.

Stosch, H.G. (1981) Sc, Cr, Co, Ni partitioning between minerals from spinel peridotite xenoliths. Contributions to Mineralogy and Petrology, 78, 166–174.

Suzuki, K. (1981) Grain boundary concentration of rare earth elements in a hornblende cumulate. Geochemical Journal, 15, 295–301.

Takahashi, E. (1980) Thermal history of lherzolite xenoliths. I. Petrology of lherzolite xenoliths from the Ichinomegata crater, Oga Peninsula, northeast Japan. Geochimica et Cosmochimica Acta, 44, 1643–1658.

Wells, P.R.A. (1977) Pyroxene thermometry in simple and complex systems. Contributions to Mineralogy and Petrology, 62, 129–139.

Wittry, D.B. (1980) Spectroscopy in microscopy and microanalysis: The search for an ultimate analytical technique. Electron Microscope, 3, 14–21.

Ziebold, T.O. (1967) Precision and sensitivity in electron microprobe analysis. Analytical Chemistry, 39, 858–861.

Manuscript received June 30, 1986
Manuscript accepted May 21, 1987